Energy Storage Materials 70 (2024) 103437

Contents lists available at ScienceDirect

Energy Storage Materials

journal homepage: www.elsevier.com/locate/ensm

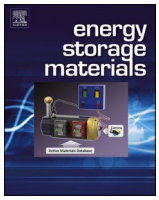

Model-based electrolyte design for near-neutral aqueous zinc batteries with manganese-oxide cathodes

Niklas J. Herrmann [a,b], Birger Horstmann [a,b,c,*]

[a] German Aerospace Center, Wilhelm-Runge-Straße 10, D-89081 Ulm, Germany
[b] Helmholtz Institute Ulm, Helmholtzstraße 11, D-89081 Ulm, Germany
[c] Universität Ulm, Albert-Einstein-Allee 47, D-89081 Ulm, Germany

ARTICLE INFO

Keywords:
Aqueous zinc-ion batteries
Continuum modeling
Electrolyte speciation
Cathode dissolution
Precipitation

ABSTRACT

Most modern zinc-ion batteries (ZIBs) with MnO_2 cathodes utilize near-neutral aqueous electrolytes based on a zinc sulfate ($ZnSO_4$) salt. They achieve good cycling stabilities with high intrinsic safety, employ environmentally friendly materials, and deliver competitive volumetric energy densities. However, the limited solubility of zinc-sulfate species influences the performance and cycling mechanism of these cells. We examine the speciation and solubility limits of $ZnSO_4$, zinc chloride ($ZnCl_2$), and zinc triflate ($Zn(CF_3SO_3)_2$) in aqueous solutions and simulate their intrinsic transport properties. We use our earlier developed and validated full-cell model to investigate the effects of several electrolytes on the two-phase cycling behavior. Previously, we reported that the origin of the second phase is based on an interaction mechanism between cathodic dissolution and a precipitation reaction at the cathode. We investigate this interplay between electrolyte stability and cathodic dissolution based on electrolyte choice. Our theory-based approach allows us to identify performance indicators of aqueous electrolytes and draws a consistent pathway to optimize electrolyte design for manganese-based ZIBs.

1. Introduction

Sustainable next-generation batteries are needed for a successful energy transition. Zinc-based batteries are stable within aqueous electrolytes and achieve excellent energy densities [1]. Zinc-metal anodes in alkaline electrolytes use a conversion mechanism to ZnO, which allows excellent energy densities. However, this conversion during cycling comes at the risk of passivation issues. Alkaline batteries with MnO_2 cathodes show an adverse effect between cycle life and depth-of discharge [2]. Yamamoto and Shoji [3,4] conducted studies of Zn-MnO_2 batteries and substituted the KOH electrolyte with near-neutral aqueous electrolytes, which drastically increased cycling life of the MnO_2 cathodes and opened the path to modern zinc-ion batteries (ZIB) [5].

Most current ZIBs utilize MnO_2 cathodes with aqueous electrolytes based on $ZnSO_4$ [1,6,7], similar to the findings of Yamamoto and Shoji in the late 80s [3,4]. $MnSO_4$ is added to additionally improve cycling life and the stability of the cathodes [8–11]. An often-reproduced argument is that the $MnSO_4$ additive decreases the dissolution mechanism of the cathode [8]. However, there is experimental evidence that $MnSO_4$ does not mitigate this mechanism but achieves better cycling stability by increasing the redeposition of MnO_2 during charging [10,12]. In our recent work, we published a theory-based approach to understanding said cycling mechanism [13]. We found that the two phases observed during discharge are associated with two dominating mechanisms. The first discharge phase can be explained by Zn^{2+}-insertion into the cathode, while the second phase is due to the dissolution of Mn^{2+} from the cathode structure. The precipitation of $Zn_4(OH)_6SO_4$ (ZHS) at the cathode plays a crucial role in mediating the transition of both phases [13,14]. While the dissolution of Mn^{2+} is a self-limiting process in the first phase, the pH buffering effect of the ZHS dissolution leads to an increasing cathodic dissolution in the second phase. However, to our knowledge, there is no systematic research on the interaction of electrolyte composition and cycling mechanism of MnO_2 cathodes.

Electrolyte additives for ZIBs serve different purposes [15]. One focus is to increase the performance of the zinc-metal anode for ZIBs [16,17]. Strategies resemble those for near-neutral zinc-air batteries, where triflate, chloride-nitrate, and other electrolytes have been successfully tested [18–20]. However, zinc-metal anodes for ZIBs should not undergo a conversion reaction but enable a Zn^{2+} transport to the cathode. Besides additives used to form artificial surface layers, zinc salt precipitation has

* Corresponding author.
E-mail address: birger.horstmann@dlr.de (B. Horstmann).

https://doi.org/10.1016/j.ensm.2024.103437
Received 1 March 2024; Received in revised form 6 April 2024; Accepted 26 April 2024
Available online 21 May 2024

been discussed as detrimental to fast insertion kinetics at the cathode [21,22]. Several approaches include electrolyte additives, which act as anode surfactant [11,23–28]. These additives are used to construct an artificial layer on the anode surface, which consists of inorganic compounds, such as fluorinated salts [23,24,29], decomposition products of organic solvents or additives [26,27], or organic and inorganic layers as a hybrid structure [25,28]. This artificial layer, similar to the SEI, which stabilizes anode performance in lithium ion[30] and lithium metal batteries[31], is shown to modify anode overpotential, achieve a beneficial surface morphology, and reduce the hydrogen evolution of the anode [17]. Another focus is on the overall kinetics of zinc metal anodes in near-neutral aqueous electrolytes [15,16,32]. Here, performance is not only influenced by zinc concentration but also by complexation, and it is found that $Zn(CF_3SO_3)2$ shows significantly reduced overpotentials compared to $ZnSO_4$ [32]. However, an electrolyte, beneficial in a half-cell setup, does not necessarily perform better in full-cell experiments.

Several electrolyte studies were conducted in full-cell experiments [33]. Historically, Shoji & Yamamoto [3,4] reported the best performance for a $ZnSO_4$ electrolyte. In the last decade, some of the original electrolytes were re-tested [34,35], as well as additional salts, especially $Zn(CF_3SO_3)_2$[5,9,25,36,37]. Electrolyte studies with manganese oxide and vanadium oxide cathodes showed that both for $Zn(CF_3SO_3)_2$[9,26,38,39] as well as for $ZnCl_2$ electrolytes [27,40], a zinc-salt precipitate was reported to form during discharge and to be dissolved again during the subsequent charge. Some experimental evidence hints that a triflate-based electrolyte might increase cycling stability [9]. Still, there is no extensive discussion of the influence of the two discharge phases and the effect on cathodic dissolution. This limits the design of a consistent optimization strategy for aqueous ZIBs with MnO_2 cathodes.

In our recent work [13], we developed a numerical model that investigates how the speciation of $ZnSO_4$ electrolytes interacts with the electrochemical stability of the MnO_2 cathode. We were able to show a unique interaction mechanism between speciation and precipitation in $ZnSO_4$ electrolytes and the stability and dissolution reaction of the cathode. With the help of numerical simulations, we deduced that the experimentally observed two-phase behavior could only be explained in the presence of a ZHS precipitation reaction.

The current paper presents a theory-driven approach to understanding the requirements of electrolyte design for high-performance ZIBs by comparing the cycling mechanisms in the $ZnSO_4$[13] electrolyte with $ZnCl_2$, $Zn(CF_3SO_3)_2$. We use electrolyte thermodynamics to investigate how the speciation differs within the electrolytes and how their speciation is influenced by different Mn^{2+} salts. We present a novel approach to evaluate the effective transference number of Zn^{2+} ions in aqueous electrolytes and simulate the electrolyte's solubility limits to highlight governing parameters based on their thermodynamically derived speciation. We use our validated full-cell model [13] to describe their dynamic behavior during cycling. Finally, we investigate how the cycling mechanism of MnO_2-based cell chemistries interacts with aqueous electrolytes beyond the commonly used $ZnSO_4$ and how their respective transport properties and solubilities influence it.

2. Theory

The transport properties and stability of aqueous electrolytes in ZIBs are based on electrolyte speciation. In our work, we solve the complex formation reactions based on electrolyte thermodynamics to describe the influence of species concentrations on the electrochemical and precipitation reactions and their effect on electrolyte transport. A coherent theory for transport in near-neutral aqueous electrolytes was previously developed for near-neutral aqueous electrolytes for zinc-air batteries [19,20,41] and adapted and validated for ZIBs [13]. In the following subsections, we shortly discuss how the electrolyte speciation is simulated (Subsection 2.1), how the electrolyte transport is influenced by the aqueous complexes formed (Subsection 2.2), and how the formed species influence the reaction rates (see Subsection 2.3).

2.1. Electrolyte speciation

Electrolyte speciation is calculated based on thermodynamic data on complex formation in aqueous solutions [42–44]. The formation of complexes in the electrolyte can be described with a set of homogeneous electrolyte reactions[45,46]. These reactions and their thermodynamic equilibrium constants are listed in the Supporting Information (Table S1, S2 and S3). We solve the complexation in these systems by using the law of mass action, which states that the ratio of reaction products and reactants is constant in equilibrium. For example for $Zn(Cl)_3^-$, the law of mass action reads

$$\frac{c_{Zn(Cl)_3^-}}{c_{Zn^{2+}}\, c_{Cl^-}{}^3} = 10^{K}\,, \tag{1}$$

with K = 0.5 from Reference [42]. We use the equilibrium quotients to rewrite the concentrations of the individual complexes as a function of their components. In the exemplary case of a $ZnCl_2$ electrolyte, these are $c_{Zn^{2+}}$, c_{Cl^-} and c_{H^+}. The proportionality relation between H+ and OH- concentration in aqueous electrolytes yields $c_{OH^-} = 10^{-14}\cdot c_{H^+}{}^{-1}$. We use this to get a set of algebraic equations for solving speciation. In a $ZnCl_2$ electrolyte, these have the form

$$c_{Zn^{2+}}{}^{T} = c_{Zn^{2+}} + \sum_i j\cdot 10^{K_i}\cdot c_{Zn^{2+}}{}^{j}\cdot c_{Cl^-}{}^{k}\cdot c_{H^+}{}^{l}\,, \tag{2}$$

$$c_{Cl^-}{}^{T} = c_{Cl^-} + \sum_i k\cdot 10^{K_i}\cdot c_{Zn^{2+}}{}^{j}\cdot c_{Cl^-}{}^{k}\cdot c_{H^+}{}^{l}\,, \text{ and} \tag{3}$$

$$c_{H^+}{}^{T} = c_{H^+} + \sum_i l\cdot 10^{K_i}\cdot c_{Zn^{2+}}{}^{j}\cdot c_{Cl^-}{}^{k}\cdot c_{H^+}{}^{l}. \tag{4}$$

Here, c_i^T are the total concentrations of the dissolved ions, irrespective of the complex the ion is bound in. j, k and l are the stochiometric amounts of Zn^{2+}, Cl^- and H^+ in complex i with the equilibrium constant K_i. These equations lead to our definitions of quasi-particles q, with

$$c_q = \sum_i \tau_{i,q} c_i\,, \tag{5}$$

where $\tau_{i,q}$ are the stochiometric contribution of species i to quasiparticle q. A definition of all quasi-particles used for the $ZnSO_4$, $ZnCl_2$, and $Zn(CF_3SO_3)_2$ electrolytes, including the Mn^{2+}-additives, can be found in Section in the Supporting Information.

Solubility in the investigated aqueous electrolyte is handled using the mass action equation for a specific precipitation reaction. In zinc-chloride electrolytes, the zinc-chloride hydroxide salt (ZHC) precipitates with [40]

$$5Zn^{2+} + 2Cl^- + 8OH^- \rightleftharpoons Zn_5(OH)_8Cl_2\downarrow. \tag{6}$$

In equilibrium, a solubility product K_{sp} exists so that

$$10^{K_{sp}} = c_{Zn^{2+}}{}^{5}\cdot c_{Cl^-}{}^{2}\cdot c_{H^+}{}^{-8}. \tag{7}$$

Here, we substituted $c_{OH^-}{}^{8} = \left(10^{-14}\right)^{8}\cdot c_{H^+}{}^{-8}$. All precipitation reactions are given in Table 1 alongside their thermodynamically derived solubility product.

The dissolution of Mn^{2+} from the cathode's structure (see Subsection 2.3) is regarded as detrimental to cycling stability. Thus, manganese salts are added in an attempt to mitigate its effect. Within the discussion of electrolyte additives, Le Chatelier's principle is used to motivate the beneficial behavior of a Mn^{2+} additive on the dissolution behavior of the cathode [15]. The common-ion effect is an application of the generalized argument from Chatelier's principle. It describes the decrease in solubility by adding an ionic additive with an ion in common with the

Table 1
Precipitation reactions in the investigated electrolytes. *The solubility product of $Zn_5(OH)_2OTf_8$is extrapolated from experimental pH measurements in zinc triflate electrolytes [48].

Electrolyte			Reaction			K_{sp}	Ref.
$ZnSO_4$	$ZnCl_2$	$Zn(CF_3SO_3)_2$					
✓			$4Zn^{2+} + SO_4^{2-} + 6OH^-$	⇌	$Zn_4(OH)_6SO_4$	28.4	[42]
	✓		$5Zn^{2+} + 2Cl^- + 8OH^-$	⇌	$Zn_5(OH)_8Cl_2$	38.5	[42]
		✓	$5Zn^{2+} + 8CF_3SO_3^- + 2OH^-$	⇌	$Zn_5(OH)_2(CF_3SO_3)_8$	16.7	[48]*
✓	✓	✓	$Zn^{2+} + 2OH^-$	⇌	$ZnO + H_2O$	11.17	[42]
✓	✓	✓	$Zn^{2+} + 2OH^-$	⇌	$Zn(OH)_2$	12.45	[42]

precipitate [47]. In the above-described system, this would apply to the addition of $MnCl_2$ to the $ZnCl_2$ electrolyte. Based on the expectation from the common-ion effect, an electrolyte with added $MnCl_2$ contains more chloride ions, which should, at first sight, reduce the Zn^{2+} solubility for the precipitation of ZHC. However, in the electrolytes investigated here, an increase in the total amount of chloride ions does not necessarily increase the amount of solvated Cl- similarly due to the formation or dissociation of complexes. We study this effect both in equilibrium simulations in Subsection 3.2 and within a dynamic cell model in Subsection 4.2.

2.2. Electrolyte transport

The electrolyte transport used in this model is based on a thermodynamically consistent transport theory[49,50]. The transport description we use here is an adaption based on our quasi-particle model [13,19,20,41] to achieve a stable solution for multi-component electrolytes. For this model, we neglect the convective contribution to the transport equation [51,52].

In a generalized concentrated solution theory approach, we can calculate the transport for each concentration c_i by solving the differential-algebraic equations[51]

$$\frac{\partial \epsilon_e c_i}{\partial t} = -\vec{\nabla}\cdot\vec{N}_i^{DM} + \dot{s}_i, \text{ and} \tag{8}$$

$$0 = -\vec{\nabla}\cdot\vec{j} + \sum_i z_i F \dot{s}_i. \tag{9}$$

Here, ϵ_e is the volume fraction of the electrolyte,z_i is the species' charge, and $\dot{s}_i$ is the species' source term. $\vec{N}_i^{DM}$ is the diffusion-migration flux and $\vec{j}$ is the current density, which are defined as

$$\vec{N}_i^{DM} = -D_i \epsilon_e^{\beta} \vec{\nabla} c_i + \frac{t_i}{z_i F}\vec{j}, \text{ and} \tag{10}$$

$$\vec{j} = -\sum_i \frac{z_i^2 F^2 D_i}{RT} c_i \vec{\nabla}\phi - \sum_i z_i F D_i \vec{\nabla} c_i. \tag{11}$$

Here, D_i is the species' diffusion coefficient, z_i is its elementary charge, and t_i is its transference number. The summand in the definition of $\vec{j}$ is equal to the species conductivity $\kappa_i = \frac{z_i^2 F^2 D_i}{RT} c_i$. The species' source term s_i includes both the source terms for the electrochemical and precipitation reactions and the complex formation reactions.

This brute-force approach yields many equations, as the transport must be solved for each species. This equation system is also highly unstable, as the complex formation is significantly faster than regular diffusion & migration timescales and may lead to rapidly changing concentrations.

We use the definition from Equation (5) to find our quasi-particle transport equation to mitigate this challenge

$$\frac{\partial \epsilon_e c_q}{\partial t} = \sum_i \tau_{i,q} \frac{\partial \epsilon_e^{\beta} c_i}{\partial t} = \sum_i \tau_{i,q} \left(-\vec{\nabla}\cdot\vec{N}_i^{DM} + \dot{s}_i \right). \tag{12}$$

We define effective transport parameters for the quasi-particles to simplify this equation. The quasi-particle diffusion coefficient reads

$$D_q = \frac{\sum_i \tau_{i,q} D_i c_i}{c_q}, \tag{13}$$

and the quasi-particle transference number

$$t_q = z_q \cdot \sum_i \frac{\tau_{i,q} t_i}{z_i}. \tag{14}$$

The transference number of the individual complexes used here is based on dilute-solution theory with

$$t_i = \frac{z_i^2 D_i c_i}{\sum_i z_i^2 D_i c_i}. \tag{15}$$

Finally, we use these definitions to rewrite the transport equation as

$$\frac{\partial \epsilon_e c_q}{\partial t} = \vec{\nabla}\cdot D_q \epsilon_e \vec{\nabla} c_q - \frac{t_q}{z_q F}\vec{j} + \dot{s}_q. \tag{16}$$

This transport equation's source term, $\dot{s}_q$, is independent of the complex formation reactions and is only influenced by electrochemical and complex formation reactions. This allows us to effectively reduce the dimensionality of the simulations while still consistently integrating the thermodynamics of the formed complexes.

2.3. Electrochemical reactions

The electrochemical reactions included in this model are the Zn/Zn^{2+} redox-reaction at the anode, as well as Zn^{2+}-insertion and Mn^{2+}-dissolution reactions at the MnO_2-cathodes. We omit other reported electrochemical reactions, especially the hydrogen evolution reaction at the anode, as those are considered detrimental side reactions, and mitigation strategies exist to avoid them. An in-detail discussion and validation of this approach can be found in our previous publication [13]. This subsection highlights the influences of the individual aqueous species on these reaction terms.

Within this work, all electrochemical reactions are calculated as a symmetric Butler-Volmer rate[53]. The generalized equation for the reaction rate k_r is given as

$$k_r = k_r^0 \sinh\left(\frac{zF}{2RT}\cdot(\Delta\phi - U_r)\right). \tag{17}$$

Here, $\Delta\phi$ is the difference in the electrical potential between electrolyte and electrode and U_r the open circuit potential of the individual reaction.

At the anode, the reaction rate of the Zn/Zn^{2+} redox reaction [54] is

calculated with an open circuit potential U_{ano} as

$$U_{ano} = U_{0,Zn} + \frac{RT}{zF}\log\frac{c_{Zn^{2+}}}{c_0}, \tag{18}$$

and the reaction rate k_r^0 is proportional to the electrolytes zinc concentration with $k_r^0 \propto \sqrt{c_{Zn^{2+}}}$. Therefore, electrolytes with a higher contribution of hydrated $c_{Zn^{2+}}$ ions, which are not bound in any ligand complex, allow faster reaction kinetics and the concentration-dependent Nernst term changes the equilibrium potential of the redox-reaction.

The insertion reaction is described with the chemical equation

$$Zn^{2+} + Mn_2O_4 + 2e^- \rightleftharpoons ZnMn_2O_4. \tag{19}$$

The rate of this insertion reaction k_{ins} is, on the one hand, influenced by the activity of hydrated Zn^{2+}, with

$$k_{ins} \propto k_0 \cdot \sqrt{SOC(1-SOC)}\sqrt{c_{Zn^{2+}}}\ , \tag{20}$$

where SOC, the state of charge, is the normalized concentration of Zn^{2+} within the cathode structure. On the other hand, the open circuit potential of the insertion reactions is given with

$$U_{ins} = U_{0,ins} + \frac{RT}{zF}\left(\log\frac{SOC}{1-SOC} + \log\frac{c_{Zn^{2+}}}{c_0}\right), \tag{21}$$

where $U_{0,ins}$ is the potential of the Zn^{2+}-insertion reaction at reference conditions. Regarding electrolyte influences, the rate of the insertion reaction changes analog to the anodic redox reaction.

Additionally, we model the electrochemical dissolution and deposition of Mn^{2+} at the cathode. In accordance with DFT calculations [13] and experimental findings [55] we describe the dissolution reaction as

$$2Zn_{0.5}MnO_2 + 2e^- + 8H^+ \rightleftharpoons Zn^{2+} + 2Mn^{2+} + 4H_2O. \tag{22}$$

The open circuit voltage of the dissolution process U_{diss} is given as

$$U_{diss} = U_{0,diss} - \frac{RT}{zF}\left[\log\left(\frac{c_{Zn^{2+}}}{c_0}\cdot\frac{c_{Mn^{2+}}{}^2}{c_0}\right) - 8\log\left(\frac{c_{H+}}{c_0}\right)\right], \tag{23}$$

and the rate for this dissolution reaction is proportional to $k_{diss}^0 \propto \sqrt{\frac{c_{Zn_{0.5}MnO_2}}{c_{Zn_{0.5}MnO_2^{max}}}}$. Therefore, the dissolution reaction is slower within electrolytes with higher free concentrations of Zn^{2+}, Mn^{2+}, or under more alkaline conditions.

3. Equilibrium simulations

This section investigates the equilibrium composition and transport parameters of different Zn^{2+}-based aqueous electrolytes. Based on the thermodynamic data of the multitude of complexes that form between Zn^{2+}, Mn^{2+}, and the anions SO_4^{2-}, Cl-, and $CF_3SO_3^-$ in an aqueous environment, we can calculate the prevalence of the individual species present. In the first subsection (Subsection 3.1), we evaluate this for a $ZnSO_4|MnSO_4$ electrolyte and compare it with a $ZnCl_2|MnCl_2$ electrolyte and a $Zn(CF_3SO_3)_2$ | $Mn(CFSO_3)_2$ electrolyte. Based on this, we analyze the behavior of the different electrolytes in a quasi-equilibrium manner. In the following subsection (Subsection 3.2), we discuss the effects of changing the regular $MnSO_4$ additive with either $MnCl_2$ or $Mn(CF_3SO_3)_2$ in a $ZnSO_4$ additive.

3.1. Ternary salt mixtures

We use an algebraic set of equations derived from the law of mass action of the complex-forming reactions (see Subsection 2.1) to solve the speciation of a 2M $ZnSO_4$ electrolyte with a 0.5M additive of $MnSO_4$ for a given pH. To allow simulating the complex formation for a fixed pH and Zn^{2+}T concentration, the concentration of the salt anion - here SO_4^{2-} - has to be implicitly calculated and is not fixed. The experimental analog of this simulation is the titration of an aqueous ZnO electrolyte with the help of H_2SO_4. Aqueous $ZnSO_4$ electrolytes are the most common choice for ZIBs [1,56]. The chosen concentration is based on experimentally validated performance [12,57,58]. A detailed discussion on the choice of this electrolyte can be found in Reference [13].

Figure 1 and 2 a) shows the concentrations of the formed Zn-complexes for a $Zn^{2+}{}_T$ concentration of 2M and 0.5M $MnSO_4$ as a function of electrolyte pH. In the pH region below the solubility limit of ZHS, the predominant complex is a $ZnSO_4$ complex with a concentration of approximately 1.45M. This $ZnSO_4$ complex therefore binds ≈ 73% of the available 2M of Zn^{2+}. At this pH region, hydrated Zn^{2+} and $Zn(SO_4)_2{}^{2-}$ contribute significantly less, with ≈ 12.5% each. The solubility limits of the different Zn-salt precipitation reactions are indicated by horizontal lines in Fig. 2 a). The governing precipitation in this electrolyte is the precipitation of $Zn_4SO_4(OH)_6$ at a pH of ≈ 5.4. The solubility limit of ZnO and $Zn(OH)_2$ is significantly higher, with 6.3 and 6.5. Complexes with OH^- are only relevant under alkaline conditions above the solubility limits of all investigated zinc salts.

Fig. 2 b) shows the transference number of the electrolyte as a function of Zn_T^{2+} concentration and pH value. Analog to Fig. 2 a), the concentration of SO_4^{2-}T is solved implicitly. The solid gray lines are trajectories of constant SO_4^{2-}T concentration. As the electrochemical reactions (Subsection 2.3) do not change the amount of sulfate, they are pathways during cycling if no precipitation reaction is present. The white circle indicates the state of a benign solution of 2M $ZnSO_4$ and 0.5M $MnSO_4$. The colored lines show the solubility limits of the precipitation reactions. The solubility of ZHS is not only limiting at a 2M concentration but remains to limit the stability of the electrolyte in the investigated range [13]. Within the stability limits of the electrolyte, the quasi-particle transference number of zinc is negative. While all species transference numbers of the individual zinc-ligand complexes are positive, the overall transference number is negative due to the composition of the quasi-particle. Due to the presence of the negatively charged $Zn(SO_4)_2^{2-}$ species, the net migration flux induced on the Zn^{2+} quasi-particle is in the opposite direction of the positively charged Zn^{2+}.

Following, we compare the speciation of the chloride- and triflate-based electrolytes with the previously discussed results for the sulfate electrolyte. Fig. 3 a) shows the predominant zinc-ligand complexes for a $ZnCl_2$ electrolyte with a Zn-concentration of $c_{Zn^{2+}}{}^T = 2M$ and 0.5M $MnCl_2$ additive. The horizontal lines indicate the solubility limit of $Zn_5(OH)_8Cl_2$ and ZnO, as well as $Zn(OH)_2$. The stability limiting

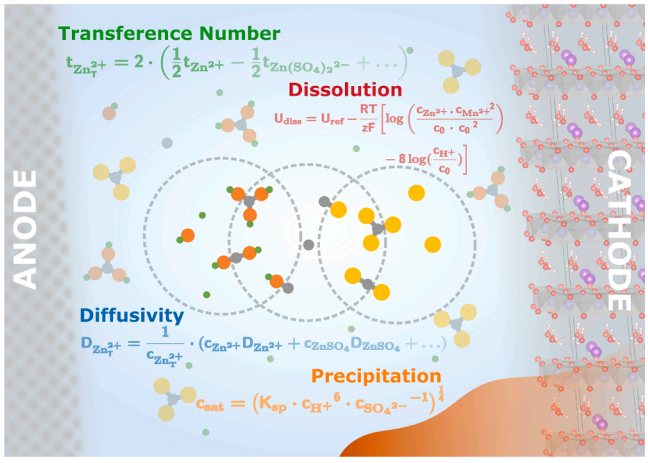

Fig. 1. Schematic figure of relevant parameters of aqueous electrolytes which influence the cycling mechanism. Shown are the governing effects that are influenced by electrolyte composition, i.e., the solubility of precipitates, dissolution potential, and the intrinsic transport properties of the electrolyte.

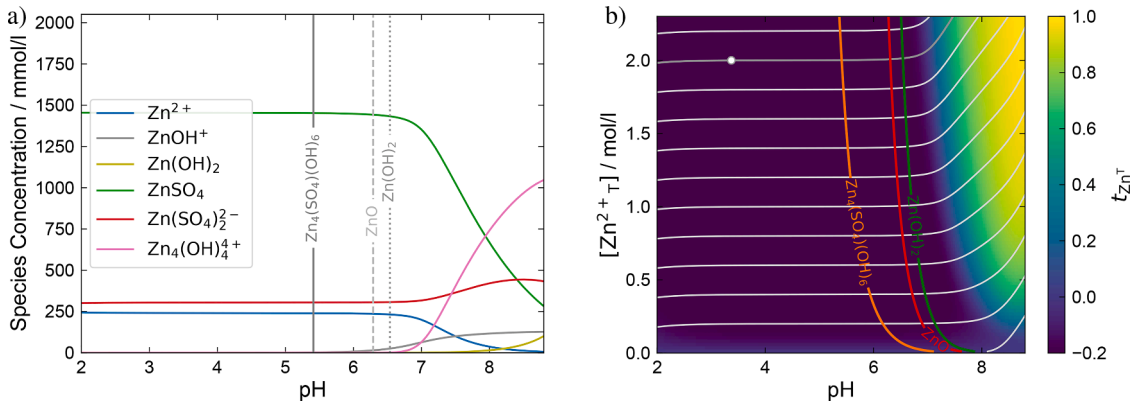

Fig. 2. a) Complex formation in a $ZnSO_4$ electrolyte with a fixed Zn amount of $c_{Zn^{2+}}{}^{T} = 2M$ and a 0.5M Mn^{2+} additive. Shown are the normalized Zn^{2+}-species concentrations as a function of pH. The horizontal gray lines indicate the solubility limit regarding the different precipitation reactions. b) Transference number of the zinc quasi-particle of the sulfate electrolyte with 0.5M Mn^{2+} additive. The gray lines show trajectories of constant SO_4^{2-} concentration. The white circle indicates the initial state of a benign solution of 2M $ZnSO_4$ with 0.5M $MnSO_4$ and the dark gray indicates its isoline, i.e. a 2.5M concentration of SO_4^{2-}. The colored lines indicate the solubility limits of the denoted species.

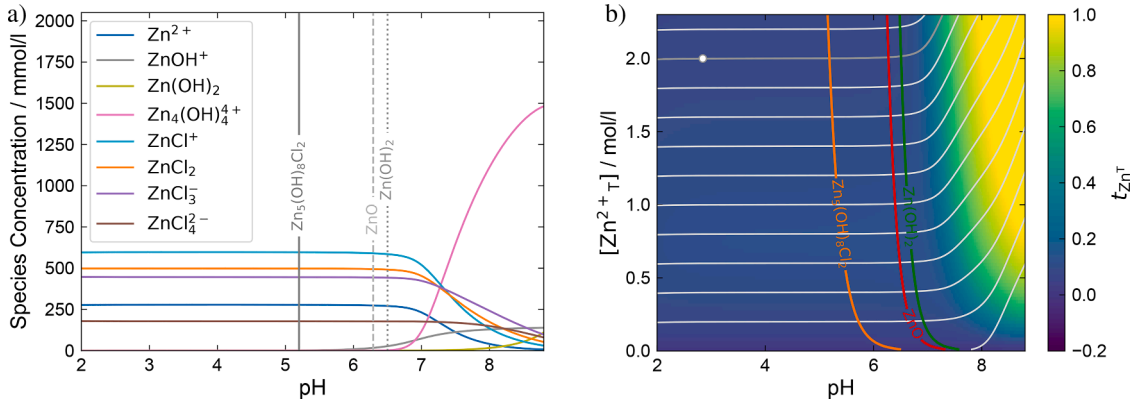

Fig. 3. a) Complex formation in a $ZnCl_2$ electrolyte with a fixed Zn amount of $c_{Zn^{2+}}{}^{T} = 2M$ and a 0.5M Mn^{2+} additive. Shown are the normalized Zn^{2+}-species concentrations as a function of pH. The horizontal gray lines indicate the solubility limit regarding the different precipitation reactions. b) Transference number of the zinc quasi-particle of the chloride electrolyte with 0.5M Mn^{2+} additive. The gray lines show trajectories of constant Cl^- concentration. The white circle indicates the initial state of a benign solution of a 2M $ZnCl_2$ with 0.5M $MnCl_2$ and the dark gray indicates its isoline, i.e. a 5M concentration of Cl^- The colored lines indicate the solubility limits of the different species.

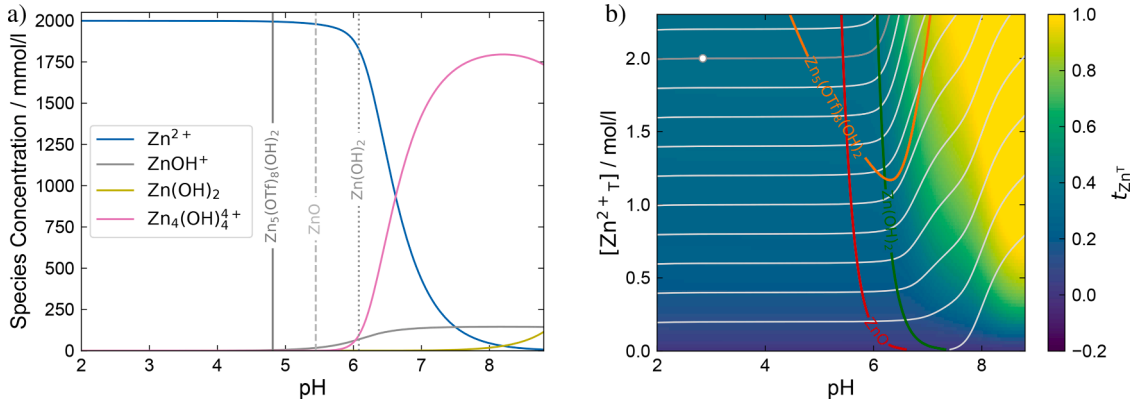

Fig. 4. a) Complex formation in a $Zn(CF_3SO_3)_2$ electrolyte with a fixed Zn amount of $c_{Zn^{2+}}{}^{T} = 2M$ and a 0.5M Mn^{2+} additive. Shown are the normalized Zn^{2+}-species concentrations as a function of pH. The horizontal gray lines indicate the solubility limit regarding the different precipitation reactions. b) Transference number of the zinc quasi-particle of the triflate electrolyte with 0.5M Mn^{2+} additive. The gray lines show trajectories of constant $CF_3SO_3^-$ concentration. The white circle indicates the initial state of a benign solution of a 2M $Zn(CF_3SO_3)_2$ with 0.5M $Mn(CF_3SO_3)_2$ an the dark gray indicates its isoline, i.e. a 5M concentration of $CF_3SO_3^-$. The colored lines indicate the solubility limits of the different species.

precipitation here is $Zn_5(OH)_8Cl_2$ at a pH of ≈ 5.2. Below the precipitation limit, relevant complexes are chloride-based of the form $Zn(Cl)_x^{2-x}$, with $ZnCl^+$ being the most prevalent and binding ≈ 32% of the available Zn^{2+} ions. In contrast to the $ZnSO_4$ electrolyte, the average charge of the zinc complexes is higher due to the monovalent chloride ion than the divalent sulfate ion.

Comparable to the results for the $ZnSO_4$-based electrolyte, the precipitation of the chloride-based zinc-salt is limiting, independent of the amount of dissolved zinc (see Fig. 3 b)). The transference number, however, is higher than within the sulfate electrolyte but is, similar to $ZnSO_4$, not sensitive to the concentration of Zn^{2+}.

The dominant zinc-ligand complexes of a $Zn(CF_3SO_3)_2$ electrolyte with a Zn-concentration of $c_{Zn^{2+}}{}^{T} = 2M$ and 0.5M $Mn(CF_3SO_3)_2$ additive are shown in Fig. 4 a). The zinc triflate is entirely dissociated below the solubility limit of $Zn_5(OH)_2(CF_3SO_3)_8$, which is also found experimentally[59,60]. Zincate species are only relevant under alkaline conditions and are not present in the operating window of ZIBs. Fig. 4 b) shows the quasi-particle transference number, solubility limits, and trajectories of constant $CF_3SO_{3T}^-$ concentration. In contrast to the behavior of the sulfate and chloride electrolytes, the solubility of $Zn_5(OH)_2(CF_3SO_3)_8$ is not limiting for all zinc concentrations. While solubility is limited by the triflate salt above concentrations of 1.5M, the pH limit gets more alkaline with decreasing zinc concentration. At low concentrations, zinc triflate is soluble independent of pH, and the electrolyte's stability is governed by the precipitation of ZnO. At alkaline conditions, the trajectories of constant $CF_3SO_{3T}^-$ concentration show a feature not observed in the chloride and sulfate electrolytes. Here, the concentration of $Zn_4(OH)_4{}^{4+}$ reaches a maximum and decreases afterward, which can be observed in the slopes of the trajectories around a pH of 8. However, it has to be noted that the complex formation on the right side of the solubility limits will not be reached during operation, as extended precipitation will buffer the pH close to the solubility limits. Therefore, these features do not directly influence the electrolyte's performance.

The zinc-quasi particle's transference number influences the electrolyte's migration-based net flux of zinc ions. Fig. 5 highlights the sensitivity of the transference number for the different electrolytes and with different MnX-additive concentrations of 0M to 0.5M, where the additive's anion X is identical with the anion of the zinc salt. To evaluate the electrolyte composition and thus the transference number in dependency of the dissolved manganese, we use the charge neutrality in the electrolyte to postulate that the change in zinc concentration and the change in manganese concentration must cancel out, i.e., $\Delta c_{Zn^{2+}{}_T} = -\Delta c_{Mn^{2+}{}_T}$. During discharge, zinc oxidation at the anode matches the charge transferred via a cathodic dissolution reaction. This approach was already used and discussed in Reference [13]. In Fig. 5, the solid lines show the transference number for the electrolytes without a manganese additive; the dashed and dotted lines are results with 0.25M and 0.5M manganese salt added. The transition between the colored and gray line indicates the electrolyte's solubility limit, as discussed in the previous paragraphs. With all electrolytes, the transference number of the zinc quasi-particle decreases with increasing manganese additive. During the dissolution of the manganese, i.e., $-\Delta c_{Mn^{2+}{}_T} > 0$, the transference number is rarely influenced. During deposition of MnO_2, the transference number slightly increases, but the influence is insignificant.

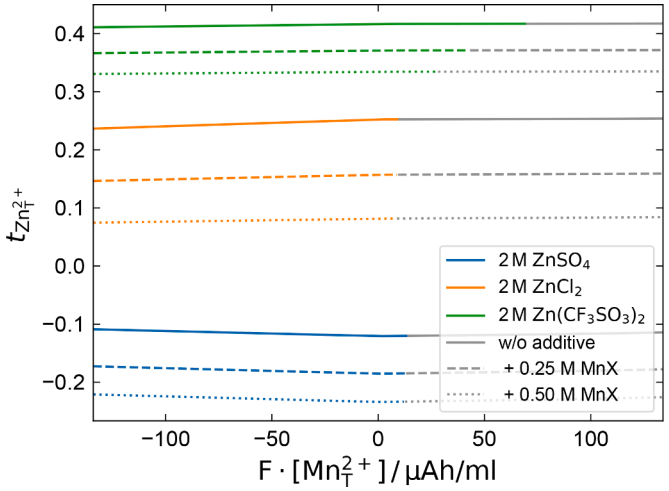

Fig. 5. The quasi-particle transference number of the Zn^{2+} quasi-particle in the investigated electrolytes. Shown are the calculated values as a function of the dissolved manganese. The different line styles indicate the amount of pre-added MnX to the solution within the range of 0M to 0.5M, where X denotes the corresponding anion to the investigated zinc salt. The relevant solubility limits are shown by the transition of color to gray lines.

The triflate-based electrolyte shows a significantly higher solubility limit compared to $ZnSO_4$ and $ZnCl_2$ in this simulation. Additionally, a common-ion effect (see Subsection 2.1) can be observed in the triflate electrolyte. The higher the amount of $Mn(CF_3SO_3)_2$ pre-added to the electrolyte, the lower the solubility limit during the dissolution reaction. As the $CF_3SO_3^-$ does not function as a ligand for the cations, the triflate ions which are added with the dissolved $Mn(CF_3SO_3)_2$ consequently lower the solubility of the $Zn_5(OH)_2(CF_3SO_3)_8$. This strong correlation can not be observed for the sulfate and chloride electrolytes.

3.2. Quaternary salt mixtures

In the previous section, we found that manganese additives can alter electrolyte transport properties and the solubility limit of zinc-hydroxide salt. We found that this can be motivated by a common-ion effect in dissociated electrolytes, such as zinc triflate, but has different behavior in zinc sulfate and zinc chloride electrolytes, which form many relevant complexes. Tuning the solubility and transference number can significantly alter the cell's behavior. Therefore, we investigate the influence of quaternary salt mixtures under equilibrium conditions and discuss if the expectations from the common-ion effect can be applied here. Instead of the commonly used choice of ternary mixtures, we investigate the mixture of zinc sulfate with either a manganese chloride or triflate additive.

Fig. 6 a) shows the transference number and solubility limits of a $ZnSO_4$ electrolyte with a 0.5M $MnCl_2$ additive. In contrast to the result for the ternary $ZnSO_4$ electrolyte (see Fig. 2), the transference number is higher, which is due to formed ZnCl complexes as shown in Figure S1. At all zinc concentrations, the solubility of $Zn_5(OH)_8Cl_2$ is higher than the limiting solubility for ZHS so that the expected precipitation remains unchanged.

Fig. 6 b) shows the identical analysis for a mixture of $ZnSO_4$ with a 0.5M $Mn(CF_3SO_3)_2$ additive. Here, we observe a quasi-particle transference number significantly higher than in the ternary zinc-manganese-sulfate electrolyte and higher than with the $MnCl_2$ additive. The triflate ion in this mixture forms neither complexes with the Mn^{2+} nor with the Zn^{2+}. Therefore, the complex formation of Mn^{2+} with SO_4^{2-} reduces the activity of sulfate in the electrolyte and thereby shifts the ratio of Zn^{2+} and $Zn(SO_4)_2{}^{2-}$ to the favor of Zn^{2+}.

Following, we investigate the influence of a second anion in sulfate-based electrolytes on ZHS solubility and compare the effects of Cl- and $CF_3SO_3^-$ within quarternary mixtures. We therefore simulate a mixture of a 2M $ZnSO_4$ and vary the additive. The additive concentration is chosen so that the manganese concentration is kept constant with $c_{Mn^{2+}{}_T} = 0.5M$ and the additive's anion is either changed from SO_4^{2-} to Cl^- or to $CF_3SO_3^-$. Fig. 7 shows the resulting equilibrium pH and the solubility limit, as well as the MnO_2 dissolution potential (see Equation (23)) for the different compositions. By introducing triflate as an additive, we find that partially substituting SO_4^{2-} with $CF_3SO_3^-$ decreases

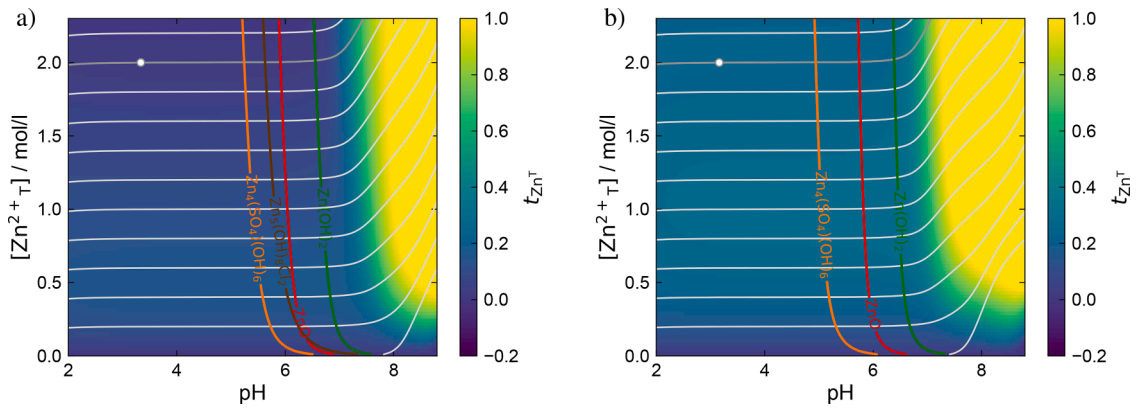

Fig. 6. Solubility Limits and Zn-Transference numbers of the quarternary electrolytes. Shown are the results for $ZnSO_4$ with an a) 0.5M $MnCl_2$ additive, and b) a 0.5M $Mn(CF_3SO_3)_2$ additive for a given total zinc concentration and electrolyte pH. The colored lines indicate the solubility limits of all relevant precipitation reactions.

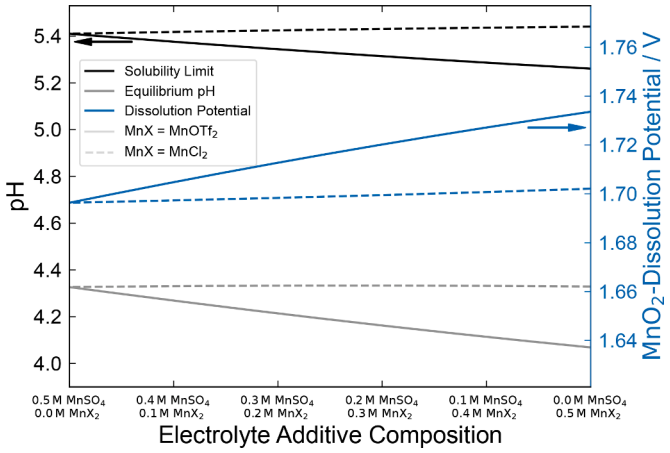

Fig. 7. Variation of electrolyte parameters in the quarternary transition. Shown are the results for salt mixtures with a constant concentration of 2M Zn^{2+} and.5M Mn^{2+}. The total anion concentration of SO_4^{2-} starts at 2.5M and the anion of the.5M Mn^{2+} salt is then gradually replaced by either $X = Cl^-$ (shown as dotted line) or $X = CF_3SO_3^-$ shown as. Shown are the electrolyte pH and the pH of the solubility limit for ZHS on the left axis. The right axis shows the Mn^{2+} dissolution potential.

both the pH at equilibrium from 4.3 to 4.1 as well as the projected solubility limit for this composition. The dissolution potential for the 2M $ZnSO_4$,5M $Mn(CF_3SO_3)_2$ electrolyte is 37 mV higher than within the ternary sulfate electrolyte. This change in dissolution potential is primarily a result of the more acidic conditions. The analog introduction of chloride ions does not lead to an equally significant change. Both the equilibrium pH value and the dissolution potential remain relatively constant. Only the lower concentration of SO_4^{2-} within the quarternary sulfate-chloride electrolyte slightly increases the solubility limit of ZHS. However, we find that the regular common-ion effect is not ubiquitous. A reduced solubility is observed for the $Mn(CF_3SO_3)_2$ additive. The corresponding acid of this additive, triflic acid, is a superacid and, per definition, a stronger acid than sulfuric acid and hydrochloric acid. This has the effect that the Mn^{2+} ions from the $Mn(CF_3SO_3)_2$ additive now pair with some of the sulfate anions from the zinc sulfate, effectively increasing the amount of free zinc present, thereby significantly lowering the solubility of ZHS. To conclude, the thermodynamics of the present zinc-ligand complexes must be considered when evaluating the influence of different electrolyte compositions. In the following section, we use our electrolyte model to investigate the electrolyte's influence on the cycling mechanism.

4. Cycling simulations

This section investigates the cycling behavior of the previously tested aqueous electrolytes within a dynamic electrochemical cell model. Within the previous section, we investigate solubility limits, pH stability, and the quasi-particle transference number of the electrolytes. Here, we use a physicochemical cell model to study the dynamic interaction of the electrolyte with the electrochemical electrode reactions. Analog to the simulations performed in Reference [13], we use a P2D-electrochemical model to describe transport within electrolytes and electrodes and model the electrochemical dissolution and insertion reactions and the kinetics of the precipitation reaction. The parameterization of the P2D model is a generalized set of parameters that resemble experimentally used 2032 coin cells[22,61–63], which we validated previously [13]. The complete set of parameters can be found in the Supporting Information, Section 2. The geometry of the electrodes and the separator and the kinetics of all electrochemical kinetics are identically parametrized for all electrolytes; adaptions are solely made to the kinetics of the precipitation reaction, as discussed in the Supporting Informations (Section 2).

In the first subsection (see Subsection 4.1), we present cycling results in the sulfate, chloride, and triflate-based ternary electrolytes, which we analyzed in Subsection 3.1. We examine how the quasi-particle Zn^{2+}-transference number influences cycling performance and how the two-phase behavior changes with the different dominating precipitates. In the second part (see Subsection 4.2), we investigate how the cycling behavior of the quaternary electrolytes, investigated in Subsection 3.2 differs from the ternary case. Finally, we discuss how cycling performance is influenced by the different electrolyte properties and how this can be used to optimize future aqueous ZIBs.

4.1. Ternary electrolytes

First, we investigate the influence of the dominant salt anion on the cell's performance. We simulate a galvanostatic discharge with a current density of 0.4 mA cm^{-2} within our parameterized 2032 coin cell model. At the simulated mass loading of 2 mg cm^{-2} this results in a discharge current of 200mAg^{-1}. If not explicitly stated otherwise, this discharge current density is also applied for other simulations, and all displayed results show the behavior in the second discharge or cycle. In experimental works, the first discharge significantly differs from the subsequent cycling behavior. Our cell model only consists of reversible reactions, so this deviation can not be appropriately described. Our procedure resembles experimental protocols by performing an initialization cycle and analyzing the cycle afterward.

In this subsection, we simulate cycling in 2M $ZnSO_4$ + 0.5M $MnSO_4$,

2M $ZnCl_2$ + 0.5M $MnCl_2$ and 2M $Zn(CF_3SO_3)_2$ + 0.5M $Mn(CF_3SO_3)_2$ electrolytes. Fig. 8 a) shows the simulated discharge behavior. The colored regions beneath the discharge curve indicate the fractional contribution of the Zn^{2+}-insertion and Mn^{2+}-dissolution reactions. The lower right axis of Fig. 8 a) shows the total discharged capacity of the two processes for the different electrolytes. At the beginning of the discharge, i.e., the first discharge phase, all electrolytes show solely a Zn^{2+} insertion mechanism. Later, the cells transition to a second discharge phase with present Mn^{2+}-dissolution and show a more or less pronounced voltage dip, associated with nucleation/salt precipitation [13,54,64]. However, the chloride electrolyte increases the dissolution-precipitation mechanism compared to the sulfate electrolyte. In contrast, the triflate-based electrolyte's second discharge phase is barely present. A quantitative evaluation of the individual capacities of both the Zn^{2+}-insertion as well as the Mn^{2+} dissolution reaction is shown on the lower right axis of Fig. 8.

Fig. 8 b) shows the pH evolution in the electrolyte and the volume fraction of the precipitate during the galvanostatic discharge. We find that the pH of all electrolytes becomes more alkaline during the first phase of the discharge. With the onset of the precipitation reaction, the pH drops shortly. During the second phase of the discharge, the pH increases slower in the chloride and sulfate electrolytes; in the triflate-based electrolyte, the pH rises considerably quicker. The precipitation of ZHS, as well as ZHC and $Zn_5(OH)_2(CF_3SO_3)_8$, is only observed during the second discharge phase. Here, the sulfate and chloride-based electrolytes show a similar amount of formed precipitate. The triflate-based electrolyte shows less precipitation, but the growth rate is significantly higher, correlating with the faster increase in pH value. The precipitation reaction is limited to the vicinity of the cathode for all electrolytes, as shown in Figure S3, S4 and S5. We conclude that the general two-phase mechanism we described for ZIBs with conventional $ZnSO_4$ electrolytes is not limited to this specific electrolyte but can also be observed in other aqueous electrolytes. However, the quantitative influence of the Mn^{2+}-dissolution mechanism not only depends on Mn^{2+}-concentration, as reported in Reference [13] but also on the anion and thus the different aqueous zinc complexes and precipitates formed.

Now, we study the rate performance for the different electrolytes. Therefore, we galvanostatically cycle the cells as mentioned above at different current densities from 100mAg^{-1} up to 10A g^{-1}. Fig. 9 i) to iii) show the cell potentials during the discharge and subsequent charge for a selection of simulated rates. The lower right axis displays the energy available during the discharge as a function of the applied rate. In the sulfate electrolyte, the second discharge phase is only present at low discharge rates[13]. The prolonged second phase for the chloride electrolyte is more stable at higher rates but will disappear above a certain

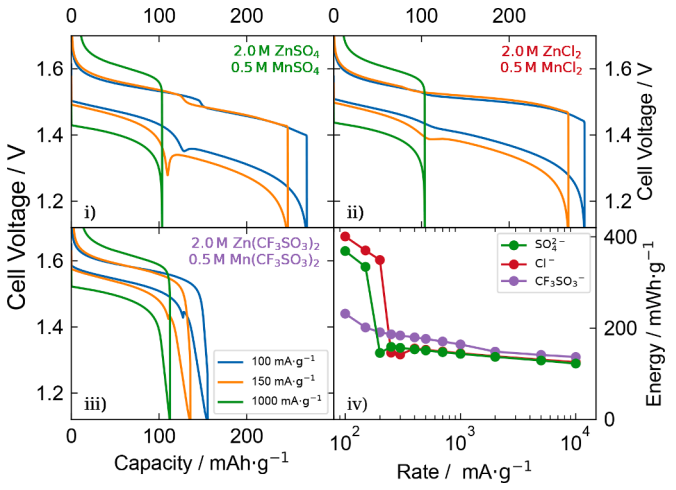

Fig. 9. i)-iii) Galvanostatic cycling behavior behavior for discharge rates between 100mAg^{-1} and 10A g^{-1} in sulfate, chloride and triflate-based ternary electrolytes. iv) Comparison of the discharged energy content as a function of discharge current.

threshold. On the other hand, the results of Fig. 9 iii) show that the discharge in $Zn(CF_3SO_3)_2$ electrolytes only shows a minimal second phase, which is further suppressed at a higher rate. This fits well with the experimental results from Zhang et al. [9] Additionally, the discharged capacity shows a much smaller relative decrease. Fig. 9 iv) shows the achievable gravimetric energy density during discharge. Here, the triflate electrolyte performs better at rates where the second discharge phase is kinetically suppressed. The suppression of the second discharge phase leads to a rapid decay of achievable capacity above a threshold rate for the sulfate and chloride electrolyte; this sharp drop can not be observed in the triflate electrolyte as the second discharge phase does not contribute significantly to the total capacity. To conclude, we find that the kinetics of the second phase differ significantly between the different electrolytes. While the kinetics of sulfate and chloride electrolytes are roughly similar, the triflate electrolyte shows precipitation and a second phase with a cathodic dissolution but to a significantly smaller extent. However, triflate-based electrolytes perform better in the Zn^{2+} insertion phase and during cycling at higher rates. We attribute the improved high-rate performance of the triflate electrolyte to the large quasi-particle transference number (see Subsection 3.1).

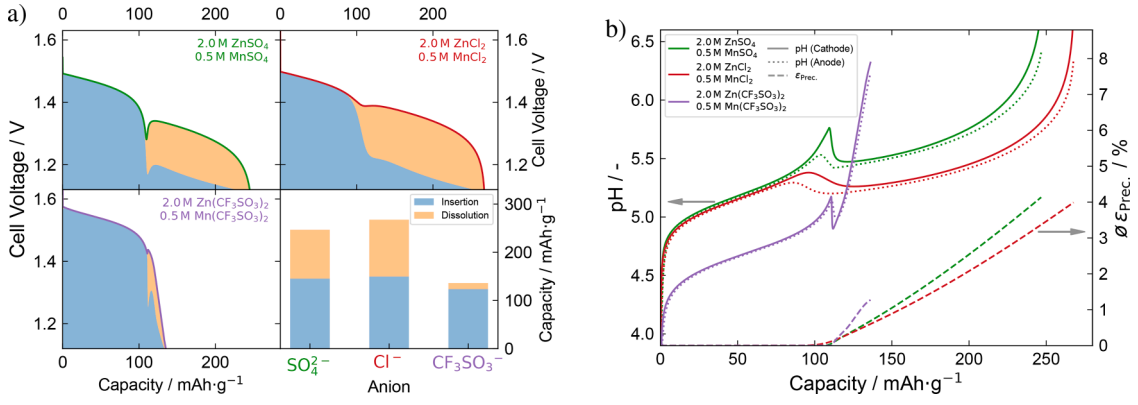

Fig. 8. a) Galvanostatic discharge behavior at 200 mAg^{-1} (equal to 0.4mA cm^{-2} at the simulated mass loading of 2mgcm^{-2}) for different ternary electrolytes. Shown are the simulated cell voltages during the discharge. The colored areas below the discharge potential represent the fractional contribution of the Zn^{2+}-insertion current and Mn^{2+}-dissolution current to the overall cell current. b) Evolution of pH at the electrodes during discharge. The electrolyte pH at both anode and cathode and the average volume-fraction of zinc-salt precipitate in the cell are shown.

4.2. Quarternary electrolytes

In this subsection, we study the influence of a quarternary electrolyte on the cathodic dissolution and precipitation reactions within our P2D cell model. We test mixtures based on a 2M $ZnSO_4$ electrolytes with a 0.5M manganese additive. An analysis of the equilibrium behavior of these quarternary electrolytes is shown in a previous section (see Subsection 3.2). We compare the conventionally used $MnSO_4$ additive with $Mn(Cl)_2$ and $Mn(CF_3SO_3)_2$. Fig. 10 a) shows the result for a simulated galvanostatic discharge at 200mAg^{-1} analog to the results from Fig. 8 a). With the addition of 0.5M $MnSO_4$, a clear separation of the two phases can be observed. In Reference [13], we discussed that the higher the amount of $MnSO_4$ additive, the longer the first discharge phase and the later the onset of precipitation. The dissolution reaction onsets much earlier in the discharge for the tested chloride and triflate-based electrolytes. However, if discharged until 1.1V, the difference in total capacity from the Mn^{2+} dissolution reaction does not differ a lot (lower right axis).

Fig. 10 b) shows the electrolyte's pH and volume fraction of the precipitate as a function of the discharged capacity. In the first discharge phase, the pH evolution of the regular and sulfate-chloride electrolyte are almost identical. However, the pH drop associated with the precipitation onset in the quarternary electrolyte is earlier and slower than in the regular sulfate electrolyte. The pH of the sulfate-triflate mixture is more acidic than the others, which is in accordance with the equilibrium results from Subsection 3.2. The growth of ZHS, shown on the right axis, indicates the earlier onset of ZHS growth in electrolytes with triflate and chloride additives. But we also observe that the amount of ZHS produced is roughly independent of the choice of Mn^{2+} additive.

4.3. Discussion

The simulation results for the different electrolytes show significant differences in characteristic cell potential and achievable capacities. This demonstrates the significance of complex formation for cell performance. For aqueous ZIBs with manganese cathodes, the electrolyte composition directly influences the interplay of the two discharge phases. The zinc-hydroxide salt precipitation is needed to transition from the first to the second discharge phase [13]. In $ZnSO_4$, this is the precipitation of ZHS, and all other tested electrolytes show a similar behavior. However, we find that the extent of the second discharge phase, dominated by the dissolution of Mn^{2+} from the cathode, is influenced by the stoichiometry of the precipitate. While ZHS and ZHC both bind 6 to 8 hydroxide per precipitated Zn^{2+}, the dominant precipitate in the triflate, $Zn_5(OH)_2(CF_3SO_3)_8$, only binds 0.5 OH- per Zn^{2+}. This significantly reduces the buffering effect and the capacity of the Mn^{2+} dissolution phase. While the Mn^{2+} dissolution phase increases achievable capacity at low rates, it is commonly regarded as partially irreversible and assumed to reduce cycle life[13]. Therefore, the reduced dissolution phase in the triflate electrolyte might help achieve higher cycling stability.

Additionally, we simulated the electrolyte transport, focusing on the quasi-particle transference number. A higher effective transference number of the Zn^{2+} species supports the zinc transport between the electrodes by increasing the migration flux (see Figure S6). The addition of Mn^{2+} to the electrolyte lowers the transference number of the Zn^{2+} quasi-particle for all ternary electrolytes, which is detrimental for Zn^{2+} transport between the electrodes. However, a Mn^{2+}-additive is needed to prolong the first discharge phase [13]. Therefore, the longer first phase brings a reduced Zn^{2+} transference number as a trade-off in the ternary electrolytes. Within the quarternary electrolytes, which achieve higher transference numbers of zinc at the same manganese content, the combination of solubility limit and Mn^{2+} dissolution potential (see Subsection 3.2) still results in a reduced first phase. We find that the reduced formation of zinc-ligand complexes in the $Zn(CF_3SO_3)_2$ electrolytes achieves the highest transference number (see Fig. 5), which transfers to a better performance at high current densities (see Fig. 9). We conclude that electrolyte design for high-performance aqueous ZIBs must be based on analyzing relevant solubility limits reactions and the formation of zinc-ligand complexes. Precipitation and formed complexes directly influence electrolyte transport and alter the cycling mechanism by interaction with the MnO_2 dissolution process and the feedback process between dissolution and zinc-hydroxide-salt precipitation. Electrolytes, such as zinc triflate, which show high zinc transference numbers and reduced precipitation, are expected to achieve better stability at low rates and reduce the transport-based overpotential at high rates.

This simulation study and the above-discussed optimization approach focus on the interaction of the cathode's cycling mechanism and the unique interaction mechanism between the cathodic dissolution of Mn^{2+} and the precipitation of zinc salts. To our knowledge, this approach has not been pursued experimentally. Electrolyte optimization strategies often focus on the stability of zinc metal anodes and decreasing anodic hydrogen evolution. For example, the usage of non-aqueous polar solvents effectively mitigates hydrogen evolution. However, the performance of MnO_2 cathodes significantly decreases in the absence of water. Recently, hybrid solvent mixtures of water with polar aprotic solvents achieved promising performance in combination with a

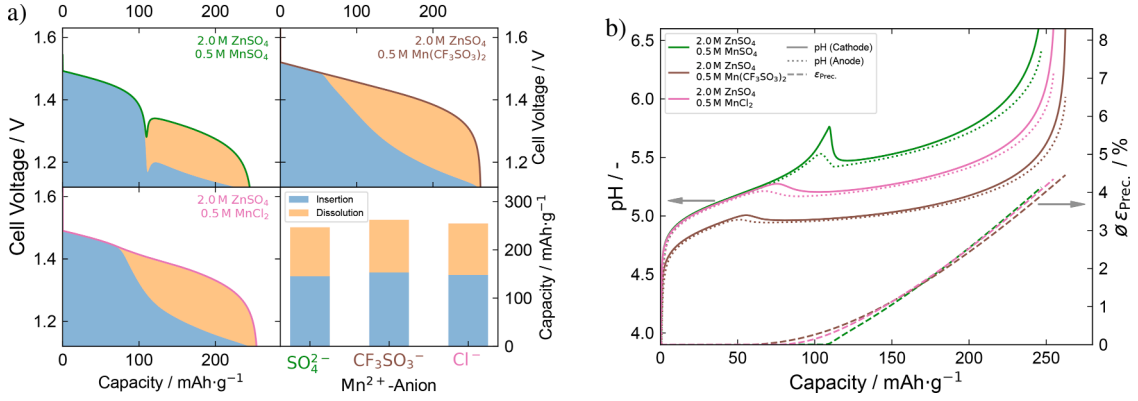

Fig. 10. a) Galvanostatic discharge behavior at 200mAg^{-1} for a 2M $ZnSO_4$ electrolytes with different Mn-salts added. Shown are the simulated cell voltages during the discharge in the second cycle. The colored areas below the discharge potential represent the fractional contribution of the Zn^{2+}-insertion current and the Mn^{2+}-dissolution current. The axis on the lower right shows the cumulative capacities of the insertion and dissolution process during discharge. b) Evolution of pH at the electrodes and for the tested electrolytes. The electrolyte pH at both anode and cathode and the average volume-fraction of Zinc-salt precipitate in the cell are shown.

zinc triflate salt [60,65,66]. This underlines that our electrolyte strategy to optimize the cycling mechanism of MnO_2 cathodes can likely be combined with optimization strategies focussing on the zinc metal anode.

5. Conclusion

Our previous work highlighted the unique mechanism leading to the observed two-phase mechanism in ZIBs with MnO_2 cathodes[13]. Within the first phase, the cathode dissolution is self-limiting due to its strong dependency on electrolyte pH. Once the electrolytes reach their precipitation limit, the electrolyte pH is buffered by a precipitation reaction so that the second phase onsets, which shows a relevant amount of cathodic dissolution and precipitation. Here, we first calculated speciations for different electrolytes, once a chloride-based electrolyte and a triflate-based one, and compared this to the commonly used sulfate-based electrolyte. We found limiting precipitation reactions similar to the ZHS precipitation in $ZnSO_4$ in all investigated mixtures. However, the electrolytes differ in Zn speciation and thus vary in the transference number of the corresponding quasi-particle. Additionally, the different stoichiometries of the precipitation reactions change the strength of the buffering effect. We showed that the different electrolytes produce inherently different results during cycling simulations, which we link with their equilibrium speciation. The quasi-particle transference number and the stochiometry and solubility of the specific precipitation reaction at the cathode significantly alter the second discharge phase. While the results for the chloride electrolytes resemble the findings for the sulfate electrolyte, the triflate electrolyte shows a significantly higher quasi-particle transference number for Zn^{2+}, which yields faster transport and a reduced influence of the second phase, expected to increase cycling stability. Knowledge of this mechanism helps design high-performance electrolytes that optimize the characteristic precipitation reaction and the cathodic dissolution. We expect that a strategy that effectively combines a $Zn(CF_3SO_3)_2$ electrolyte with additional measures to stabilize the electrodes' side-reactions catalyzed by the triflate anion increases the performance of next-generation aqueous ZIBs significantly.

CRediT authorship contribution statement

Niklas J. Herrmann: Writing – original draft, Visualization, Validation, Software, Methodology, Investigation, Formal analysis. **Birger Horstmann:** Writing – review & editing, Supervision, Resources, Project administration, Methodology, Investigation, Funding acquisition, Conceptualization.

Declaration of competing interest

The authors declare that they have no known competing financial interests or personal relationships that could have appeared to influence the work reported in this paper.

Acknowledgments

The authors acknowledge support from the Helmholtz Association and the German Research Foundation (DFG) through Grant No. INST 40/467-1 FUGG (JUSTUS cluster). The research leading to these results has received funding from the Federal Ministry of Education and Research (BMBF) in the framework of the project 'ZIB' (FKZ 03XP0204A).

Supplementary material

Supplementary material associated with this article can be found, in the online version, at 10.1016/j.ensm.2024.103437

References

[1] N. Borchers, S. Clark, B. Horstmann, K. Jayasayee, M. Juel, P. Stevens, Innovative zinc-based batteries, J. Power Sources 484 (2021) 229309, https://doi.org/10.1016/j.jpowsour.2020.229309.https://linkinghub.elsevier.com/retrieve/pii/S0378775320315974
[2] K. Kordesch, M. Weissenbacher, Rechargeable alkaline manganese dioxide/zinc batteries, J. Power Sources 51 (1994) 61–78, https://doi.org/10.1016/0378-7753(94)01955-X.
[3] T. Yamamoto, T. Shoji, Rechargeable zn|SO_4| Mno_2-type cells, Inorganica Chimica Acta 117 (1986) L27–L28, https://doi.org/10.1016/S0020-1693(00)82175-1.
[4] T. Shoji, M. Hishinuma, T. Yamamoto, Zinc-manganese dioxide galvanic cell using zinc sulphate as electrolyte. Rechargeability of the cell, J. Appl. Electrochem. 18 (1988) 521–526.
[5] C. Xu, B. Li, H. Du, F. Kang, Energetic zinc ion chemistry: the rechargeable zinc ion battery, Angewandte Chemie Int. Edit. 51 (2012) 933–935, https://doi.org/10.1002/anie.201106307.
[6] M. Song, H. Tan, D. Chao, H.J. Fan, Recent advances in zn-ion batteries, Adv. Funct. Mater. 28 (2018) 1802564, https://doi.org/10.1002/adfm.201802564.
[7] Y. Xu, G. Zhang, J. Liu, J. Zhang, X. Wang, X. Pu, J. Wang, C. Yan, Y. Cao, H. Yang, W. Li, X. Li, Recent advances on challenges and strategies of manganese dioxide cathodes for aqueous zinc-ion batteries, Energy Environ. Mater. 6 (2023) e12575, https://doi.org/10.1002/EEM2.12575.
[8] H. Pan, Y. Shao, P. Yan, Y. Cheng, K.S. Han, Z. Nie, C. Wang, J. Yang, X. Li, P. Bhattacharya, K.T. Mueller, J. Liu, Reversible aqueous zinc/manganese oxide energy storage from conversion reactions, Nature Energy 1 (2016) 16039, https://doi.org/10.1038/nenergy.2016.39.
[9] N. Zhang, F. Cheng, J. Liu, L. Wang, X. Long, X. Liu, F. Li, J. Chen, Rechargeable aqueous zinc-manganese dioxide batteries with high energy and power densities, Nature Commun. 8 (2017) 405, https://doi.org/10.1038/s41467-017-00467-x.
[10] X. Shen, X. Wang, Y. Zhou, Y. Shi, L. Zhao, H. Jin, J. Di, Q. Li, Highly reversible aqueous zn – Mno_2 battery by supplementing Mn^{2+}-mediated Mno_2 deposition and dissolution, Adv. Funct. Mater. 31 (2021) 2101579, https://doi.org/10.1002/ADFM.202101579.
[11] Z. Li, Y. Li, X. Ren, Y. Zhao, Z. Ren, Z. Yao, W. Zhang, H. Xu, Z. Wang, N. Zhang, Y. Gu, X. Li, D. Zhu, J. Zou, Elucidating the reaction mechanism of Mn^{2+} electrolyte additives in aqueous zinc batteries, Small (2023), https://doi.org/10.1002/SMLL.202301770.
[12] V. Soundharrajan, B. Sambandam, S. Kim, S. Islam, J. Jo, S. Kim, V. Mathew, Y.-k. Sun, J. Kim, The dominant role of Mn^{2+} additive on the electrochemical reaction in $ZnMn_2O_4$ cathode for aqueous zinc-ion batteries, Energy Storage Mater. 28 (2020) 407–417, https://doi.org/10.1016/j.ensm.2019.12.021.
[13] N.J. Herrmann, H. Euchner, A. Groß, B. Horstmann, The cycling mechanism of manganese-oxide cathodes in zinc batteries: a theory-based approach, Adv. Energy Mater. 14 (2024), https://doi.org/10.1002/aenm.202302553.
[14] L. Godeffroy, I. Aguilar, J. Médard, D. Larcher, J.M. Tarascon, F. Kanoufi, Decoupling the dynamics of zinc hydroxide sulfate precipitation/dissolution in aqueous Zn – Mno_2 batteries by operando optical microscopy: a missing piece of the mechanistic puzzle, Adv. Energy Mater. 12 (2022) 2200722, https://doi.org/10.1002/aenm.202200722.
[15] Y. Geng, L. Pan, Z. Peng, Z. Sun, H. Lin, C. Mao, L. Wang, L. Dai, H. Liu, K. Pan, X. Wu, Q. Zhang, Z. He, Electrolyte additive engineering for aqueous zn ion batteries, Energy Storage Mater. 51 (2022) 733–755, https://doi.org/10.1016/j.ensm.2022.07.017.https://linkinghub.elsevier.com/retrieve/pii/S2405829722003907
[16] M. Tribbia, G. Zampardi, F. La Mantia, Towards the commercialization of rechargeable aqueous zinc ion batteries: the challenge of the zinc electrodeposition at the anode, Curr. Opin. Electrochem. 38 (2023) 101230, https://doi.org/10.1016/J.COELEC.2023.101230.
[17] Q. Zhang, J. Luan, Y. Tang, X. Ji, H. Wang, Interfacial design of dendrite-free zinc anodes for aqueous zinc-ion batteries, Angew. Chemie Int. Edit. 59 (2020) 13180–13191, https://doi.org/10.1002/ANIE.202000162.
[18] W. Sun, F. Wang, B. Zhang, M. Zhang, V. Küpers, X. Ji, C. Theile, P. Bieker, K. Xu, C. Wang, M. Winter, A rechargeable zinc-air battery based on zinc peroxide chemistry, Science 371 (2021) 46–51, https://doi.org/10.1126/SCIENCE.ABB9554.
[19] S. Clark, A. Latz, B. Horstmann, Rational development of neutral aqueous electrolytes for zinc-air batteries, ChemSusChem 10 (2017) 4735–4747, https://doi.org/10.1002/cssc.201701468.
[20] S. Clark, A.R. Mainar, E. Iruin, L.C. Colmenares, J.A. Blázquez, J.R. Tolchard, Z. Jusys, B. Horstmann, Designing aqueous organic electrolytes for zinc-air batteries: method, simulation, and validation, Adv. Energy Mater. 10 (2020) 1903470, https://doi.org/10.1002/aenm.201903470.
[21] D.Y. Putro, M.H. Alfaruqi, S. Islam, S. Kim, S. Park, S. Lee, J.-Y. Hwang, Y.-K. Sun, J. Kim, Quasi-solid-state zinc-ion battery based on α – Mno_2 cathode with husk-like morphology, Electrochimica Acta 345 (2020) 136189, https://doi.org/10.1016/j.electacta.2020.136189.https://linkinghub.elsevier.com/retrieve/pii/S0013468620305818
[22] H. Chen, C. Dai, F. Xiao, Q. Yang, S. Cai, M. Xu, H.J. Fan, S. Bao, Reunderstanding the reaction mechanism of aqueous zn-mn batteries with sulfate electrolytes: role of the zinc sulfate hydroxide, Adv. Mater. (2022) 2109092, https://doi.org/10.1002/adma.202109092.
[23] L. Cao, D. Li, T. Pollard, T. Deng, B. Zhang, C. Yang, L. Chen, J. Vatamanu, E. Hu, M.J. Hourwitz, L. Ma, M. Ding, Q. Li, S. Hou, K. Gaskell, J.T. Fourkas, X.-Q. Yang, K. Xu, O. Borodin, C. Wang, Fluorinated interphase enables reversible aqueous zinc

battery chemistries, Nature Nanotechnol. 16 (2021) 902–910, https://doi.org/10.1038/s41565-021-00905-4.
[24] J. Han, H. Euchner, M. Kuenzel, S.M. Hosseini, A. Groß, A. Varzi, S. Passerini, A thin and uniform fluoride-based artificial interphase for the zinc metal anode enabling reversible Zn/Mno_2 batteries, ACS Energy Lett. 6 (2021) 3063–3071, https://doi.org/10.1021/acsenergylett.1c01249.
[25] D. Li, L. Cao, T. Deng, S. Liu, C. Wang, Design of a solid electrolyte interphase for aqueous zn batteries, Angewandte Chemie Int. Edit. 60 (2021) 13035–13041, https://doi.org/10.1002/anie.202103390.
[26] Z. Tao, Y. Zhu, Z. Zhou, A. Wang, Y. Tan, Z. Chen, M. Yu, Y. Yang, Constructing hydrophobic interface with close-packed coordination supramolecular network for long-cycling and dendrite-free zn-metal batteries, Small 18 (2022), https://doi.org/10.1002/smll.202107971.
[27] R. Yao, L. Qian, Y. Sui, G. Zhao, R. Guo, S. Hu, P. Liu, H. Zhu, F. Wang, C. Zhi, C. Yang, A versatile cation additive enabled highly reversible zinc metal anode, Adv. Energy Mater. 12 (2) (2022), https://doi.org/10.1002/AENM.202102780.
[28] H. Jiang, L. Tang, Y. Fu, S. Wang, S.K. Sandstrom, A.M. Scida, G. Li, D. Hoang, J. J. Hong, N.-C. Chiu, K.C. Stylianou, W.F. Stickle, D. Wang, J. Li, P.A. Greaney, C. Fang, X. Ji, Chloride electrolyte enabled practical zinc metal battery with a near-unity coulombic efficiency, Nature Sustainab. 6 (2023) 806–815, https://doi.org/10.1038/s41893-023-01092-x.
[29] R. Wang, Q. Ma, L. Zhang, Z. Liu, J. Wan, J. Mao, H. Li, S. Zhang, J. Hao, L. Zhang, C. Zhang, An aqueous electrolyte regulator for highly stable zinc anode under 35 to 65°C, Adv. Energy Mater. 13 (2023), https://doi.org/10.1002/AENM.202302543.
[30] B. Horstmann, F. Single, A. Latz, Review on multi-scale models of solid-electrolyte interphase formation, Curr. Opin. Electrochem. 13 (2019) 61–69, https://doi.org/10.1016/j.coelec.2018.10.013.https://linkinghub.elsevier.com/retrieve/pii/S2451910318301686
[31] B. Horstmann, J. Shi, R. Amine, M. Werres, X. He, H. Jia, F. Hausen, I. Cekic-Laskovic, S. Wiemers-Meyer, J. Lopez, D. Galvez-Aranda, F. Baakes, D. Bresser, C.-C. Su, Y. Xu, W. Xu, P. Jakes, R.-A. Eichel, E. Figgemeier, U. Krewer, J. M. Seminario, P.B. Balbuena, C. Wang, S. Passerini, Y. Shao-Horn, M. Winter, K. Amine, R. Kostecki, A. Latz, Strategies towards enabling lithium metal in batteries: interphases and electrodes, Energy Environ. Sci. 14 (2021) 5289–5314, https://doi.org/10.1039/D1EE00767J.
[32] N. Zhang, F. Cheng, Y. Liu, Q. Zhao, K. Lei, C. Chen, X. Liu, J. Chen, Cation-deficient spinel $ZnMn_2O_4$ cathode in zn(CF 3 SO 3) 2 electrolyte for rechargeable aqueous zn-ion battery, J. Am. Chem. Soc. 138 (2016) 12894–12901, https://doi.org/10.1021/jacs.6b05958.
[33] Y. Wang, Z. Wang, F. Yang, S. Liu, S. Zhang, J. Mao, Z. Guo, Electrolyte engineering enables high performance zinc-ion batteries, Small 18 (2022), https://doi.org/10.1002/SMLL.202107033.
[34] L. Zhang, I.A. Rodr-guez-Pérez, H. Jiang, C. Zhang, D.P. Leonard, Q. Guo, W. Wang, S. Han, L. Wang, X. Ji, Zncl2 "water-in-salt" electrolyte transforms the performance of vanadium oxide as a zn battery cathode, Adv. Funct. Mater. 29 (2019) 1902653, https://doi.org/10.1002/adfm.201902653.
[35] T. Wei, Q. Li, G. Yang, C. Wang, Pseudo-zn-air and zn-ion intercalation dual mechanisms to realize high-areal capacitance and long-life energy storage in aqueous zn battery, Adv. Energy Mater. 9 (2019) 1901480, https://doi.org/10.1002/aenm.201901480.
[36] W. Qiu, Y. Li, A. You, Z. Zhang, G. Li, X. Lu, Y. Tong, High-performance flexible quasi-solid-state zn − MnO_2 battery based on MnO_2 nanorod arrays coated 3d porous nitrogen-doped carbon cloth, J. Mater. Chem. A 5 (2017) 14838–14846, https://doi.org/10.1039/C7TA03274A.
[37] X. Zeng, J. Liu, J. Mao, J. Hao, Z. Wang, S. Zhou, C.D. Ling, Z. Guo, Toward a reversible mn^{4+}/Mn^{2+} redox reaction and dendrite-free zn anode in near-neutral aqueous Zn/MnO_2 batteries via salt anion chemistry, Adv. Energy Mater. 10 (2020), https://doi.org/10.1002/AENM.201904163.
[38] S.J. Kim, D. Wu, L.M. Housel, L. Wu, K.J. Takeuchi, A.C. Marschilok, E.S. Takeuchi, Y. Zhu, Toward the understanding of the reaction mechanism of Zn/MnO_2Batteries using non-alkaline aqueous electrolytes, Chem. Mater. 33 (18) (2021) 7283–7289, https://doi.org/10.1021/acs.chemmater.1c01542.
[39] P. Oberholzer, E. Tervoort, A. Bouzid, A. Pasquarello, D. Kundu, Oxide versus nonoxide cathode materials for aqueous Zn batteries: an insight into the charge storage mechanism and consequences thereof, ACS Appl. Mater. Interfaces 11 (1) (2019) 674–682, https://doi.org/10.1021/acsami.8b16284.
[40] L. Qian, W. Yao, R. Yao, Y. Sui, H. Zhu, F. Wang, J. Zhao, C. Zhi, C. Yang, Cations coordination-regulated reversibility enhancement for aqueous Zn-Ion battery, Adv. Funct. Mater. 31 (40) (2021) 2105736, https://doi.org/10.1002/adfm.202105736.
[41] S. Clark, A.R. Mainar, E. Iruin, L.C. Colmenares, J.A. Blázquez, J.R. Tolchard, A. Latz, B. Horstmann, Towards rechargeable zinc-air batteries with aqueous chloride electrolytes, J. Mater. Chem. A 7 (2019) 11387–11399, https://doi.org/10.1039/C9TA01190K.
[42] J.W. Ball, D.K. Nordstrom, User's manual for WATEQ4f, with revised thermodynamic data base and test cases for calculating speciation of major, trace, and redox elements in natural waters, U.S. Geol. Surv. Water-Resour. Investigat. Rep. 91-183 (1991) 1–188.http://wwwbrr.cr.usgs.gov/projects/GWC_chemtherm/pubs/wq4fdoc.pdf
[43] C.F. R. S. Baes, Mesmer, The Hydrolysis of Cations, John Wiley & Sons, 1976.
[44] I. Grenthe, J. Fuger, R.J.M. Konings, R.J. Lemire, A.B. Muller, C. Nguyen-Trung, Chemical Thermodynamics of Uranium, NUCLEAR ENERGY AGENCY, 2004.
[45] J.L. Limpo, A. Luis, Solubility of zinc chloride in ammoniacal ammonium chloride solutions, Hydrometallurgy 32 (1993) 247–260, https://doi.org/10.1016/0304-386X(93)90028-C.
[46] J.L. Limpo, A. Luis, M.C. Cristina, Hydrolysis of zinc chloride in aqueous ammoniacal ammonium chloride solutions, Hydrometallurgy 38 (1995) 235–243, https://doi.org/10.1016/0304-386X(94)00075-E.
[47] P. Atkins, J. de Paula, J. Keeler, Atkins' Physical Chemistry, 11, Oxford University Press, 2017.
[48] X. Liu, H. Euchner, M. Zarrabeitia, X. Gao, G.A. Elia, A. Groß, S. Passerini, Operando ph measurements decipher h + /zn 2+ intercalation chemistry in high-performance aqueous zn/δ-v 2 o 5 batteries, ACS Energy Lett. 5 (2020) 2979–2986, https://doi.org/10.1021/acsenergylett.0c01767.
[49] A. Latz, J. Zausch, Thermodynamic consistent transport theory of li-ion batteries, J. Power Sources 196 (2011) 3296–3302, https://doi.org/10.1016/J.JPOWSOUR.2010.11.088.
[50] M. Schammer, B. Horstmann, A. Latz, Theory of transport in highly concentrated electrolytes, J. Electrochem. Soc. 168 (2021) 026511, https://doi.org/10.1149/1945-7111/abdddf.
[51] J. Stamm, A. Varzi, A. Latz, B. Horstmann, Modeling nucleation and growth of zinc oxide during discharge of primary zinc-air batteries, J. Power Sources 360 (2017) 136–149, https://doi.org/10.1016/j.jpowsour.2017.05.073.
[52] F. Kilchert, M. Lorenz, M. Schammer, P. Nürnberg, M. Schönhoff, A. Latz, B. Horstmann, A volume-based description of transport in incompressible liquid electrolytes and its application to ionic liquids, Phys. Chem. Chem. Phys. 25 (2023) 25965–25978, https://doi.org/10.1039/D2CP04423D.
[53] A. Latz, J. Zausch, Thermodynamic derivation of a butler-volmer model for intercalation in li-ion batteries, Electrochimica Acta 110 (2013) 358–362, https://doi.org/10.1016/j.electacta.2013.06.043.
[54] T. Schmitt, T. Arlt, I. Manke, A. Latz, B. Horstmann, Zinc electrode shape-change in secondary air batteries: a 2d modeling approach, J. Power Sources 432 (2019) 119–132, https://doi.org/10.1016/j.jpowsour.2019.126649.
[55] X. Guo, J. Zhou, C. Bai, X. Li, G. Fang, S. Liang, Zn/MnO_2 battery chemistry with dissolution-deposition mechanism, Mater. Today Energy 16 (2020) 100396, https://doi.org/10.1016/j.mtener.2020.100396.https://linkinghub.elsevier.com/retrieve/pii/S2468606920300150
[56] L. Kang, M. Cui, Z. Zhang, F. Jiang, Rechargeable aqueous zinc-ion batteries with mild electrolytes: a comprehensive review, Batteries Supercaps 3 (2020) 966–1005, https://doi.org/10.1002/batt.202000060.
[57] M. Chamoun, W.R. Brant, C.W. Tai, G. Karlsson, D. Noréus, Rechargeability of aqueous sulfate zn/MnO_2 batteries enhanced by accessible Mn^{2+} ions, Energy Storage Mater. 15 (2018) 351–360, https://doi.org/10.1016/j.ensm.2018.06.019.
[58] S. Park, G. An, Improvement of structural stability of cathode by manganese additive in electrolyte for zinc-ion batteries, Int. J. Energy Res. 46 (2022) 8464–8470, https://doi.org/10.1002/er.7687.
[59] Z. Liu, S.Z. El Abedin, F. Endres, Raman and FTIR Spectroscopic Studies of 1-Ethyl-3-methylimidazolium Trifluoromethylsulfonate, its Mixtures with Water and the Solvation of Zinc Ions, ChemPhysChem 16 (5) (2015) 970–977, https://doi.org/10.1002/cphc.201402831.
[60] Y. Dong, L. Miao, G. Ma, S. Di, Y. Wang, L. Wang, J. Xu, N. Zhang, Non-concentrated aqueous electrolytes with organic solvent additives for stable zinc batteries, Chem. Sci. 12 (2021) 5843–5852, https://doi.org/10.1039/D0SC06734B.
[61] H. Yang, W. Zhou, D. Chen, J. Liu, Z. Yuan, M. Lu, L. Shen, V. Shulga, W. Han, D. Chao, The origin of capacity fluctuation and rescue of dead mn-based zn-ion batteries: a mn-based competitive capacity evolution protocol, Energy Environ. Sci. 15 (2022) 1106–1118, https://doi.org/10.1039/D1EE03547A.
[62] M.H. Alfaruqi, J. Gim, S. Kim, J. Song, J. Jo, S. Kim, V. Mathew, J. Kim, Enhanced reversible divalent zinc storage in a structurally stable α − MnO_2 nanorod electrode, J. Power Sources 288 (2015) 320–327, https://doi.org/10.1016/j.jpowsour.2015.04.140.
[63] H. Ren, J. Zhao, L. Yang, Q. Liang, S. Madhavi, Q. Yan, Inverse opal manganese dioxide constructed by few-layered ultrathin nanosheets as high-performance cathodes for aqueous zinc-ion batteries, Nano Res. 12 (2019) 1347–1353, https://doi.org/10.1007/s12274-019-2303-1.
[64] B. Horstmann, T. Danner, W.G. Bessler, Precipitation in aqueous lithium-oxygen batteries: a model-based analysis, Energy Environ. Sci. 6 (2013) 1299, https://doi.org/10.1039/c3ee24299d.
[65] W. Kao-ian, J. Sangsawang, P. Kidkhunthod, S. Wannapaiboon, M. Suttipong, A. Khampunbut, P. Pattananuwat, M.T. Nguyen, T. Yonezawa, S. Kheawhom, Unveiling the role of water in enhancing the performance of zinc-ion batteries using dimethyl sulfoxide electrolyte and the manganese dioxide cathode, J. Mater. Chem. A 11 (2023) 10584–10595, https://doi.org/10.1039/D3TA01014G.
[66] S.R. Motlagh, R. Khezri, M. Etesami, A.A. Mohamad, P. Kidkhunthod, M.K. Yaakob, M. Suttipong, M.T. Nguyen, T. Yonezawa, K. Nootong, S. Kheawhom, Mitigating water-related challenges in aqueous zinc-ion batteries through ether-water hybrid electrolytes, Electrochimica Acta 468 (2023) 143122, https://doi.org/10.1016/j.electacta.2023.143122.